Proceedings of GPPS Forum 18
Global Power and Propulsion Society
Montreal, 7th-9th May 2018
www.gpps.global

GPPS-2018-0025

NUMERICAL PREDICTION OF THE NOTCH EFFECT OF RIBLETS ON AXIAL COMPRESSOR BLADES

Lennart Alexander Mähler
formerly Leibniz Universität Hannover
Hannover, Lower Saxony, Germany

Tobias Willeke
Institute of Turbomachinery and Fluid Dynamics
Leibniz Universität Hannover
willeke@tfd.uni-hannover.de
Hannover, Lower Saxony, Germany

Joerg R. Seume
Institute of Turbomachinery and Fluid Dynamics
Leibniz Universität Hannover
seume@tfd.uni-hanover.de
Hannover, Lower Saxony, Germany

ABSTRACT

Riblet structured surfaces can reduce the aerodynamic drag of bodies, which are immersed in fluid flows. A future application of these microscopic grooves with dimensions below 100 µm on axial compressor blades could increase the compressor efficiency and could reduce the fuel consumption and CO_2 emissions of aircraft engines.

In order to reduce the aerodynamic wall shear stress, riblets are aligned with the flow direction. In the case of an axial compressor rotor blade, this means that the riblets are also oriented perpendicular to the radial direction of the centrifugal blade load.

Thus, the negative consequence from riblet structuring of an axial compressor rotor blade is a local stress increase by a notch factor between 1.5 and 14.0. For the example of an axial compressor rotor blade rotating at a speed of 18,000 rpm, this means, that if static strength requirements must be met, and the blade material does not have any blade internal residual stresses – like in the case of trapezoidal riblet manufactured by contact-free laser ablation – only the upper 20% of the blade span can be structured wit riblets.

INTRODUCTION

In response to an increasing global air traffic, the Advisory Council for Aeronautics Research in Europe (ACARE) published ambitious goals: CO_2 emissions of aircraft engines should be reduced by 75%, NO_x emissions by 90%, and noise has to be cut by 65% until 2050 with respect to the emission levels of the year 2000 (European Commission, 2011).

In order to achieve these goals, secondary flows in the axial compressor have to be reduced, which contribute up to 50% to the total aerodynamic loss in an aircraft engine gas turbine (Gümmer, 2000). The remaining pressure loss due to secondary flows can be reduced by active and passive measures. When reducing the amount of secondary flows, it is expected that the share of the profile loss in the total loss will increase simultaneously (Lietmeyer, 2013). The profile loss, which in a subsonic flow is a combination of friction loss and wake mixing loss, results from the boundary layer, which develops in the stream-wise direction along the blade surface.

A process, to reduce the boundary layer friction must act nearest to the blade surface in the region of highest flow gradients. In this area, the turbulent boundary layer consists of coherent vortex structures. These coherent eddies form complex flow structures, which meander over the surface.

Aerodynamicists have generally focused on the promising aerodynamic stress reduction capabilities of riblets when introducing riblets to future turbomachinery designs. Nevertheless, these small grooves are oriented perpendicular to the main loading direction. This raises serious questions about the stress increasing notch effect of riblets, and the design evaluation of a riblet structured compressor blade in terms of the aerodynamic benefits on the one hand, and the risk of losing the highly-valuable blade on the other hand.

For reasons of operational safety, the notch effect of riblets on highly loaded axial compressor blades has to be quantified and balanced against the aerodynamic effect. With the aim of evaluating the riblet potential for aerodynamic improvements in a multistage high-speed axial compressor, the authors had to quantify the riblet notch effect on a purely numerical level in order to meet safety requirements prior to experimental test runs.

This paper presents their attempt to numerically predict the stress increasing notch effect of riblets on axial compressor blades with the help of the Finite Element Analysis (FEA). For this reason, virtual tensile stress tests on grooved material samples from titanium alloy Ti6Al4V and aluminium alloy EN AW 7075 are conducted to build a database of stress concentration factors for various riblet configurations. With this database, relationships are established between the riblet shape and dimensions and the predicted stress-concentration

factor, which are finally applied to the static stress analysis of riblet structured compressor rotor blades.

FLUID MECHANICS OF RIBLETS

In order to reduce friction loss, multiple fluid dynamic investigations have been conducted with riblets on plates (Sawyer and Winter, 1987), wings or airfoils (Lietmeyer et al, 2011), ship hulls, and aircraft bodies. These microscopic grooves are aligned with the main flow direction, and demonstrated a reduction of skin friction in turbulent flows up to 10% with respect to the smooth surface (Bechert et al, 1997; Choi et al., 1993).

Many results indicate that this aerodynamic riblet effect is effective in turbulent boundary layers (Saywer and Winter, 1987; Bruse et al., 1993; Choi et al., 1993; Hage, 2004). In contrast to laminar flows, turbulent flows exhibit an elevated shear stress level resulting from an additional fluid movement perpendicular to the wall. For continuity reasons, this movement is always accompanied by a lateral movement close to the wall, forming a vortex structure (Jang et al., 1986; Bechert et al, 1997).

The aerodynamic purpose of riblets is to hinder the lateral boundary layer movements in the near wall region. The interaction between the meandering vortices and the riblet tips reduces the momentum transfer to into the aerodynamic sublayer and thus reduce the wall friction. Consequently, the larger the ratio of a riblet-covered area to the total surface of an immersed body surface is, the higher will be its potential for drag and loss reduction.

Research has shown that the turbulent shear stress can be reduced by about 10% with blade-shaped riblets compared to the smooth surface case (Bechert et al., 1997). Nevertheless, this riblet geometry has a very low mechanical resistance, which makes blade-shaped riblets unsuitable for long-term operation in technical applications. Hence, triangular or trapezoidal riblets have prevailed for technical applications because of their enhanced mechanical robustness (Lietmeyer et al., 2013). These riblets can reduce the shear stress by about 4 percent (Lietmeyer et al. 2013). For the sake of consistency with previous authors, the terms “triangular riblets” and “trapezoidal riblets” are used instead of “triangular grooves” and “trapezoidal grooves”, where only the last two terms precisely describe the groove shape between adjacent riblets, rather than the riblet shape. The same inconsistency between groove and riblet is neglected for the term “riblet width”.

RIBLET GEOMETRY AND MANUFACTURING

For a maximum reduction of the aerodynamic profile loss, a flow adapted riblet geometry is crucial. Therefore, the riblet dimensions have to be designed with respect to the local flow conditions of the respective application. The wall shear stress can only be reduced if the average dimensionless diameter of the near wall eddies is larger than the dimensionless riblet width (Bechert et al., 1997). Otherwise, if the riblet spacing is larger than the characteristic eddy dimension, the eddy is embedded in the groove between adjacent riblets, the wetted surface and the friction loss increase.

In general, the riblet height or groove depth h has to be smaller than the thickness of the viscous sublayer. The optimal aspect ratio between the riblet height h and the riblet width s has been recommended to be h/s of 0.5 for axial compressor applications (Lietmeyer, 2013; Lietmeyer, 2011). For a maximum loss reduction, very sharp riblet are recommended (Bechert et al, 1997).

For compressor blades, the averaged-riblet width is less than 100 µm. These microscopic dimensions result in high demands for the manufacturing technologies like grinding or laser ablation (Oehlert and Seume, 2006; Oehlert et al., 2007; Lietmeyer et al., 2013), which are used to produce riblet structures of acceptable quality. An overview of various manufacturing processes for riblets can be found in Romans, 2014.

Manufacturing processes like grinding or laser ablation remove material from a plain surface to form the riblets, whereas riblet coating (Kordy, 2015) adds material to the underlying support structure. Riblet rolling (Romans, 2014) just reshapes the supporting body.

Though, the riblets from each of these manufacturing processes can be taken as notches, which increase the local stress in the material, the respective manufacturing process can add additional internal residual stresses to the structured material, which might (over-)compensate the increased tensile stress from the riblet notch effect. These manufacturing techniques like rolling or grinding, which add additional residual stress to the material, rely on strong surface contact forces during manufacturing, which lead to a local material plastification from contact pressure, and to the positive effects on the dynamic fatigue behaviour, similar to intentionally shot-peened surfaces. Recently, Romans et al. (2009, 2010, 2014) presented their promising results for rolled riblet structures, where internal stresses overcompensate for the stress increasing riblet notch effect, leading to a significantly decreased high cycle fatigue of riblet structured bodies under dynamics loads.

In the present case, in which the rotor blades of an axial compressor are riblet structured by contact-free optical laser-ablation, no benefits to the fatigue resistance of the blade can be expected. This leaves the riblet-structured blade with the full consequences of increased stress levels from the riblet-notch effect. Shot peening of the blades prior or after riblet-structuring is not an option. Pre-shoot peening would result in an uneven, rough blade surface with unacceptable tolerances for the following riblet structuring. Destroying a previously riblet-structured surface by subsequent shot-peening for the sake of increased residual stresses is also not an option, because the riblet structures would be damaged by the flowing shot impacts, which are meant for adding residual material stress through strong surface deformations.

BLADE LOADS

During operation, the blades of an axial compressor are loaded with centrifugal force, aerodynamic forces, and thermal loads, all of which can be either static or dynamically changing with time. Stator blades, which by definition do not rotate, do not experience the high centrifugal loads of the rotor blades and thus have a higher strength reserve than rotor blades of similar shape and dimensions. In rotor blades, the highest load contribution results from the amount of centrifugal forces (Cumpsty, 1991; Bräunling, 2015). These centrifugal forces lead to tensile stresses in the blade material, which have to be taken into account when designing riblets for compressor rotor blades.

During steady-state operation, the static centrifugal forces are combined with blade vibrations, which might be of a self-excited or forced-response nature (Cumpsty, 1991; Grieb, 2009). Early studies of blade vibrations modelled axial blades in terms of the beam theory. Thus, complex blade vibration modes are still being classified by their basic eigenmodes and their respective combinations (Cumpsty, 1991). These basic eigenmodes are bending, torsional, and edgewise modes.

For minimum engine weight and maximum operational flexibility, compressor blades are designed not for maximum, but for sufficient fatigue strength. When structuring these blades with riblets, their stress level is increased by the notch effect. This means that in the notch between adjacent riblets local tensile stress peaks will occur. These localized stress peaks result in local material plastification, which supports crack initiation and crack propagation leading to an undesirable detachment of blade fragments. In order to prevent any loss of the precious riblet blades, it is necessary to analyze the notch effect for riblets of various shapes and dimensions. The gained knowledge of the local stress increase can then be applied during the design phase in order to reduce the risk of a blade failure from riblet structuring.

NOTCH EFFECT

Notches on the surface of a loaded component lead to a local stress peak by concentrating the uniform force distribution in an unnotched body. This results in a three-axis stress condition with normal and shear stress components. In order to perform a strength analysis, these multiaxial stress states must be reduced to an equivalent one-dimensional stress state, because material parameters like the yield stress are determined under uni-directional loading conditions. For ductile materials like Ti6Al4V and EN AW 7075, the von-Mises stress (equation 1) is recommended for the equivalent uniaxial stress state (Young and Budynas, 2002).

$$\sigma_{vM} = \sqrt{\frac{[(\sigma_1 - \sigma_2)^2 + (\sigma_2 - \sigma_3)^2 + (\sigma_3 - \sigma_1)^2]}{2}} \qquad (1)$$

Multiple notches like adjacent riblet grooves influence each other's notch effect through the stress curve overlapping. Thus, in the case of multiple notches, different regularities occur than for isolated single notches. This means that the stress concentration factors of multiple notches have to be considered in their entirety (Daryusi, 2009).

The stress concentration factor K_t quantifies the local stress increase in form of equation 1. For a linear-elastic material behaviour, it is the ratio of the maximum local stress σ_{max} in the notch and the nominal stress σ_n:

$$K_t = \frac{\sigma_{max}}{\sigma_n}. \qquad (2)$$

For the nominal stress σ_n, either the stress in the smallest cross section of the component can be used, which is called the *net-nominal stress* (index *N*), or the stress in the unnotched cross section can be used, which is the *gross-nominal stress* (index *G*). Figure 1 shows the difference between these two nominal stresses for a flat beam under tensile load.

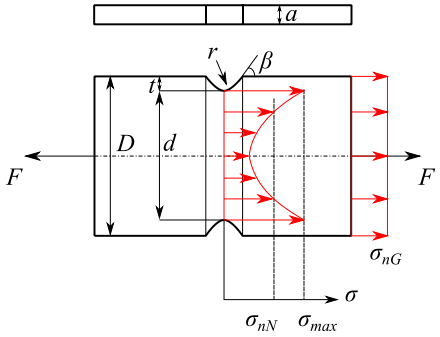

Figure 1 Notch stress in a flat bar under tension

The two definitions for the stress concentration factor are given by equations 3 and 4.

Gross-nominal formulation

$$K_{tG} = \frac{\sigma_{max}}{\sigma_{nG}} = \frac{\sigma_{max} \cdot D \cdot a}{F} \qquad (3)$$

Net-nominal formulation

$$K_{tN} = \frac{\sigma_{max}}{\sigma_{nN}} = \frac{\sigma_{max} \cdot d \cdot a}{F} \qquad (4)$$

When comparing these two equations, it is evident that the stress concentration factor, which uses the gross-nominal stress, is higher than the alternative net-nominal formulation. For the three basic loads tension, bending, and torsion, the stress concentration factor is ordered as follows (Niemann et al., 2001; Issler, 2006):

$$K_{t,tension} > K_{t,bending} > K_{t,torsional} > 1. \qquad (5)$$

In general, the notch depth t and the notch radius r have a strong influence on the stress concentration factor, whereas the notch angle β has a small influence on the stress concentration factor.

The notch effect of riblets on compressor blades has previously been determined by an FE bending beam model (Klocke et al., 2010). It was demonstrated that the stress concentration factor for this case is predominantly influenced by two geometric variables: the riblet depth and the riblet radius (Klocke et al., 2010).

An investigation according to equation 5, where the stress concentration factor is at a maximum under tensile stress has not yet been published. For this reason, this paper provides complementary values for the stress concentration factor of riblets on components under tension from static centrifugal loads.

COMPRESSOR BLADES

The impact of the riblet notch effect on blade strength is evaluated for the compressor rotor blades of a three-stage axial compressor. The compressor blades use Multiple Circular Arc (MCA) profile sections, which are radially stacked along their centers of gravity. The compressor nominal operating speed is 15,000 rpm. For static strength tests of the bladed rotor, the overspeed is set to 120 % of the nominal speed (18,000 rpm). The strength analysis is performed for this overspeed scenario using the commercial Finite Element solver Ansys Workbench 17 and the manufacturing blade geometry, which is derived from the operational (aerodynamic) geometry.

FEA RESULTS FOR PLAIN COMPRESSOR BLADES

Simulation setup

The following results are presented for the second rotor blade with an averaged blade height of 62.97 mm, and a smooth blade surface finish with no riblets. The blade root is fixed in the rotor disk dovetail joint. The blade body operates under the influence of a static centrifugal load at 18,000 rpm (figure 2). The blade materials, which are considered are Ti6Al4V and EN AW 7075. The mesh consists of 158,764 elements. Stresses are presented in the von-Mises formulation.

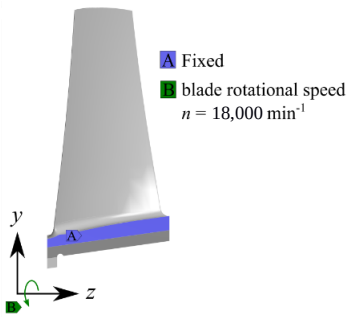

Figure 2 Boundary conditions

Von-Mises stress on the blade pressure side

Two highly loaded regions are present on the blade pressure side (figure 3). The maximum stress is located in the transition area between the blade airfoil and the blade root. High stresses occur at 50% of the chord length, and at 30% of the blade span. For the material Ti6Al4V, the stress level is higher than for EN AW 7075.

Von-Mises stress on the blade suction side

In comparison to the pressure side, the stress on the blade suction side is lower (figure 4). Stress peaks are limited to the transition area between the airfoil and the blade root.

Blade deformation

The total deformation of the blade under centrifugal load is shown in figure 5. The largest untwist takes place at the blade tip near the leading edge. The maximum deformation for EN AW 7075 is larger than for Ti6Al4V.

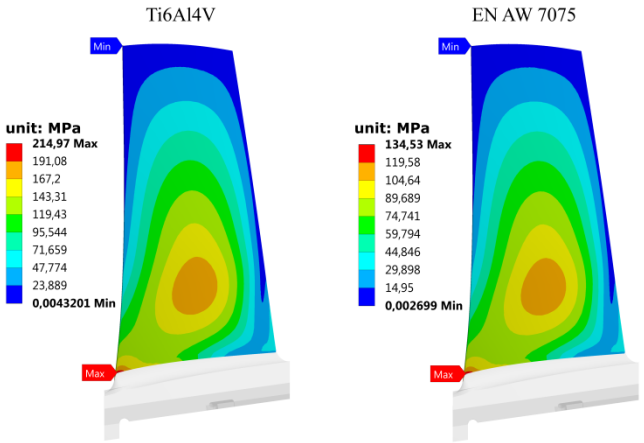

Figure 3 von-Mises stress on the pressure side of a blade from rotor row 2 at 18,000 rpm

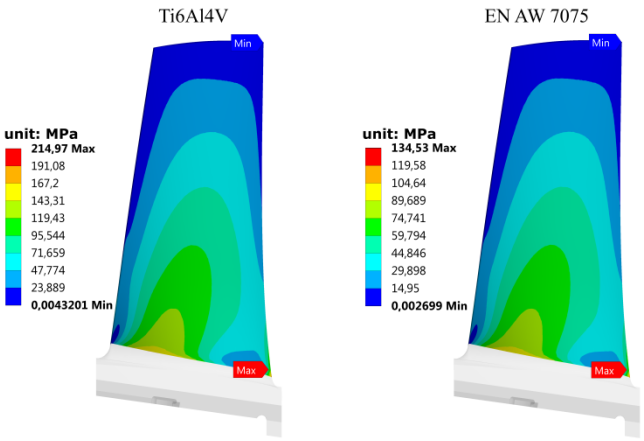

Figure 4 von-Mises stress on the suction side of a blade from rotor row 2 at 18,000 rpm

The large differences in the stress levels of the two materials results from the differences in Young's modulus and material density. The lower stress level on the blade suction side results from the convex blade shape, while the increased stress on the pressure side results from the untwisting of the concave airfoil side by the centrifugal loads. Since the blade thickness increases from the blade tip towards the blade root, and the root sections are designed for increased strength, the highest stress zones occur at the thin leading edge and around 30% of the blade span. At 30% of the blade span, the integrated centrifugal load from the upper blade sections and the varying blade thickness form a local stress maximum.

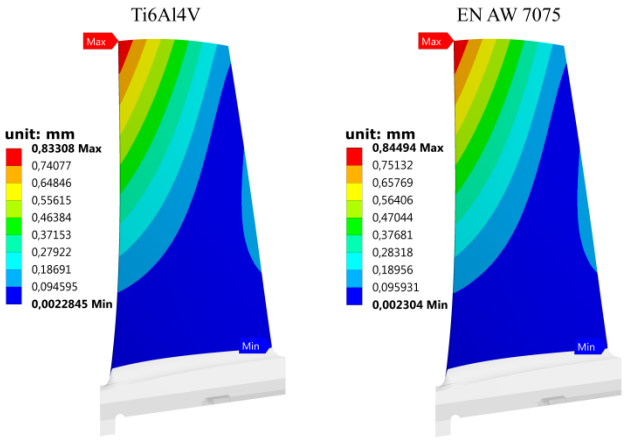

Figure 5 Total blade deformation of a blade from rotor row 2 at 18,000 rpm

The large differences in the stress levels of the two materials results from the differences in Young's modulus and material density. The lower stress level on the blade suction side results from the convex blade shape, while the increased stress on the pressure side results from the untwisting of the concave airfoil side by the centrifugal loads. Since the blade thickness increases from the blade tip towards the blade root and the root sections are designed for increased strength, the highest stress zones occur at the thin leading edge and around 30% of the blade span.

Stresses at the leading edge are higher than at the trailing edge, because of the increased blade span at the leading edge. Consequently, under the influence of rotation, a larger portion is under centrifugal load at the leading edge than at the trailing edge.

The difference in blade height is also the reason for the stronger blade untwist at the leading edge than at the trailing edge. Since the blade at the leading edge is longer than at the trailing edge, the airfoil stiffness at the leading edge is lower than at the trailing edge. The combination of an increased mass and lower stiffness results in a stronger blade untwist at the leading edge. Since the blade is fixed at its root, the deformation increases radially outwards from the hub to the tip.

RIBLET PARAMETERS AND DIMENSIONS

In order to determine the stress concentration factor for various riblet combinations, the riblet shape is parametrized by the parameters riblet width *s*, riblet height *h*, tip radius R_k, notch radius R_1, and riblet angle α (figure 6). Aerodynamically-ideal riblets would have an infinitesimally small riblet tip and a sharp transition between the riblet flanks and the groove valley. Actual riblets, which are manufactured by grinding or laser-ablation, have a round tip and a smooth transition between the riblet flanks and the groove valley.

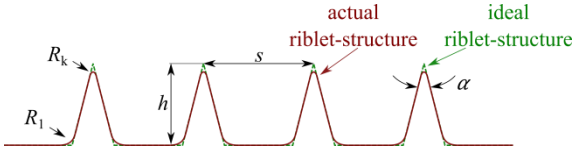

Figure 6 Riblet parameters

In the following, three different types of riblets are examined. These include the *semi-circular notch*, the *round notch* and the *trapezoidal notch* (figure 7). In order to identify specific notches in a patch of adjacent notches, the following nomenclature is introduced: the outer notches are designated as *end notches*. Notches which are adjacent to these end notches are called *after-end notches*. All internal notches between the after-end notches are grouped as *middle notches*, except for the *central notch(es)*.

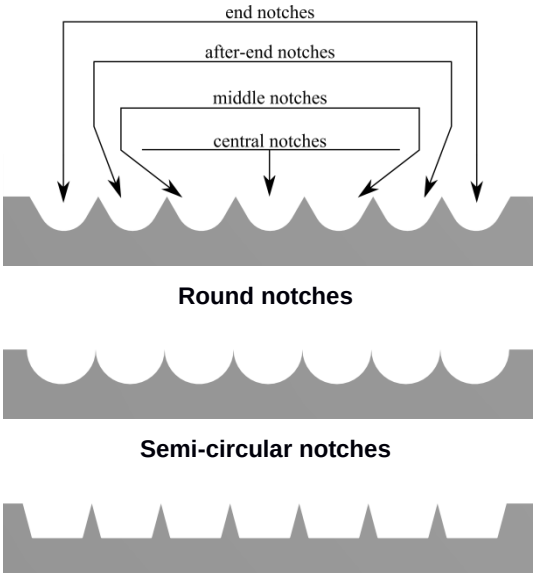

Figure 7 Riblet/notch types

The reference riblet geometry (Lietmeyer, 2003) of this study has a height-to-width ratio *h/s* of 0.5, an opening angle α of 30°, a notch radius R_1 of 1.5 µm, and a tip radius R_k of 0.15 µm. These parameters are varied to obtain different riblet shapes. It should be noted that with the parametrization of

figure 7, and with a continuous change in parameter values, the parametrized riblets can smoothly transform through all intermediate stages between the trapezoidal and the round shape (figure 7).

FEA RESULTS FOR THE RIBLET STRESS CONCENTRATION FACTOR

Procedure for the stress prediction of riblet structured axial compressor blades

In order to predict the increased stresses in a riblet structured blade, the following procedure is proposed:

1. Determine the equivalent stresses of the plain blade with ideally smooth surfaces (with no riblets).
2. Design the riblets according to aerodynamic and mechanical guidelines.
3. Determine the gross-nominal stress concentration factor of the designed riblets.
4. Scale the stress of the plain blade by the riblet stress concentration factor to obtain the stress of the riblet structured blade.

Like most strength analyses, this procedure assumes linear-elastic material behaviour. In the case of reliable and sufficient material data for crack initiation and growth, additional strength reserves from local material plastification could be included in step 3 through the use of bilinear or higher order models for the material behaviour. It should be noted that the proposed procedure can be used for both multiaxial and uniaxial stress formulation.

The advantage of this procedure is that it allows for computational inexpensive and fast design evaluations of riblet structured blades because there is no need to model and solve a blade model with all the microscopic riblet grooves on the blade surface.

Simulation setup

A virtual tensile stress test of a two-dimensional tension bar using FEA is performed in order to determine the stress concentration factor in the uniaxial stress formulation for various riblet shapes. The tension bar represents a finite cross section of the actual blade. Tension forces represent the centrifugal forces from blade rotation. The tension bar is assumed to be symmetrical along its longitudinal direction, which means that there are identical riblets on both sides of the blade, which might influence each other in regions of small blade thickness. This symmetry assumption could be replaced by different riblet structures on each side of the blade.

In order to avoid interfering influences on the notch effect from close force boundary conditions at the beam's ends, the beam length is chosen to be sufficiently large such that the beam's ends are far away from the riblet structures. The bar height represents the blade thickness and is varied in order to represent riblets at different positions between the blade leading and trailing edge.

The mesh is refined locally in the notch valleys. The validation with published experimental results (Young and Budynas, 2002) for a notched bar with a semi-circular notch shape, prove that this mesh density gives a model error of 0,33% with respect to the experimental results of Young and Budynas (2002).

Effects of the riblet shape and the number of adjacent grooves on the stress concentration factor

The influences of the riblet shape (semi-circular, round, trapezoidal, figure 7) on the stress concentration factor are determined for a beam with a reference thickness of 2 mm.

The stress concentration factor for semi-circular riblets with a width s of 60 µm and a height h of 30 µm are shown in figure 8. The maximum stress concentration factor of 3.06 is found for a single notch. When the number of adjacent riblets increases, the stress concentration factor decreases. In a patch of multiple riblets, the highest stress concentration factor is located in the end notches. For an increasing number of riblets, the stress concentration factor in the end notches approaches a limit of 2.39. Compared to a single notch, this corresponds to a reduction by 21.9% by increasing the number of riblets from 1 to 80. Likewise, the stress concentration factor for the central notches approaches a limit of 1.70. A number of 80-1 adjacent riblets is considered to be a sufficient representative of a blade surface, which is completely covered with riblets.

Figure 9 shows the stress concentration for round riblets (s: 60 µm, h: 30 µm, α: 30°, R_1: 1.5 µm, R_k: 0.15 µm). The maximum stress concentration factor of 3.12 is found for a single notch. The decreasing trend in the stress concentration factor for an increasing number of adjacent riblets results in stress concentration factors of 2.43 and 1.73 for the end notches and the central notches, respectively.

For the trapezoidal riblet shape (s: 60 µm, h: 30 µm, α: 30°, R_1: 1.5 µm, R_k: 0.15 µm, figure 10), the stress concentration factor for a single notch is 7.00, whereas the lower limit for the end notches is 6.00, and 2.28 for the central notches.

Effect of the notch radius on the stress concentration factor

The prediction of the notch radius e.g. groove radius influence on the stress concentration factor was carried out for the trapezoid notches only. The baseline design has riblets with a width s of 100 µm, a height h of 50 µm, and an opening angle α of 30°. For increasing notch radii, the stress concentration factors for a single riblet groove and two adjacent riblet grooves approach a limit of 4 (figure 11).

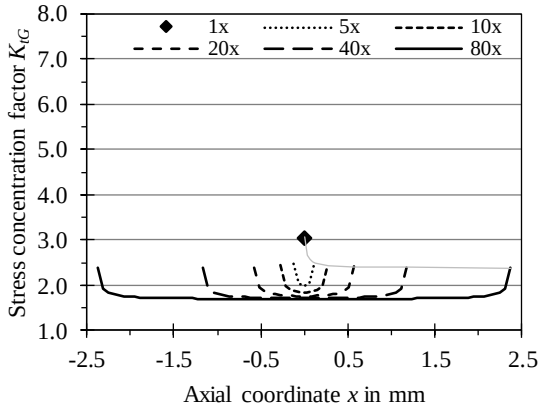

Figure 8 Stress concentration factor for semi-circular riblets

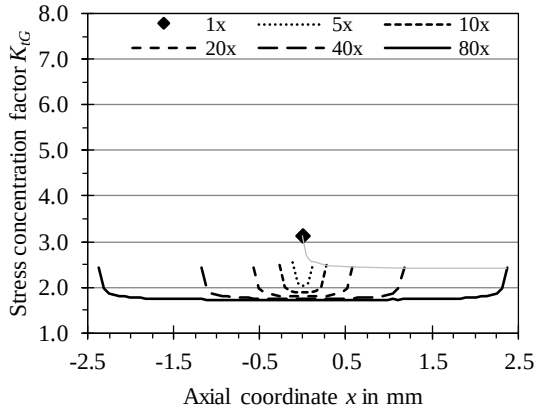

Figure 9 Stress concentration factor for round riblets

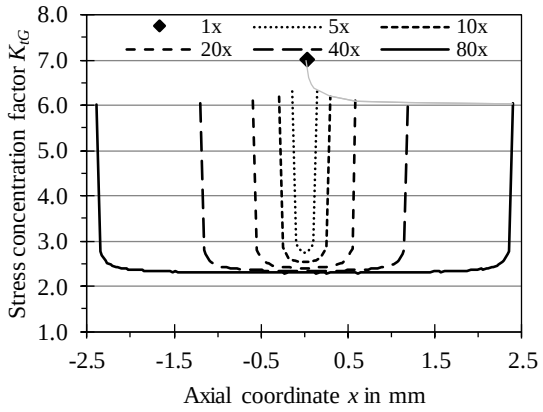

Figure 10 Stress concentration factor for trapezoidal riblets

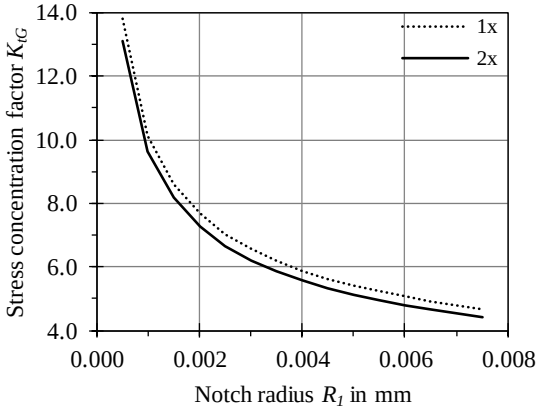

Figure 11 Stress concentration factor for trapezoidal riblets and various notch radii

Effect of the riblet height on the stress concentration factor

The influence of the riblet height is presented for all three riblet shapes. The riblets have a width s of 100 µm, a height h of 50 µm, and an angle of 30 degrees. The trapezoidal shape has a notch radius R_1 of 1.5 µm.

Semi-circular riblets show no significant changes in the stress concentration factor for varying riblet height e.g. riblet aspect ratio (figure 12). As can be seen from figure 8, an increasing number of adjacent riblets reduce the stress concentration factor.

Additionally, round riblets do not show significant changes in the stress concentration factor over the variation of the riblet height (figure 13). Nevertheless, the stress concentration factor slightly increases with an increasing riblet height.

Trapezoidal riblets show significant changes in the stress concentration factor over the variation of the riblet width (figure 14). Increasing the height by a factor of 8 results in increasing stress concentration factor by a factor of 2.5.

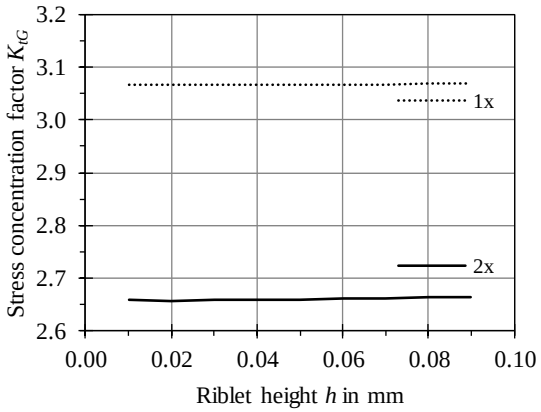

Figure 12 Stress concentration factor for semi-circular riblets and various riblets heights

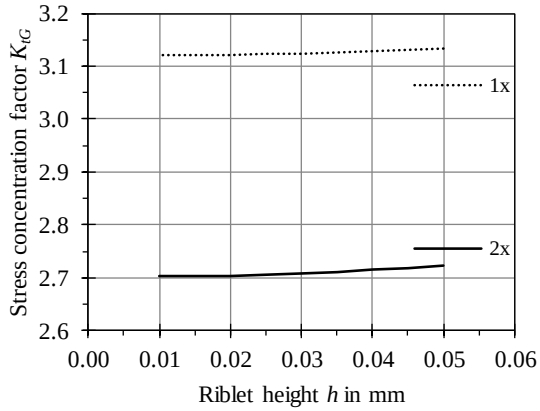

Figure 13 Stress concentration factor for round riblets and various riblets heights

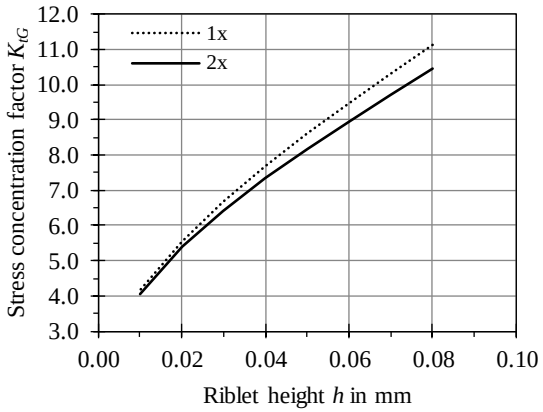

Figure 14 Stress concentration factor for trapezoidal riblets and various riblets heights

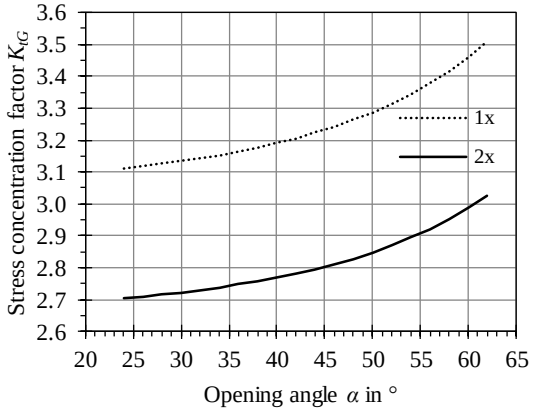

Figure 15 Stress concentration factor for round riblets and various riblets angles

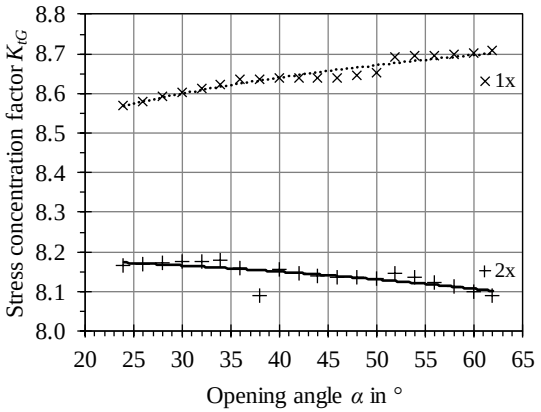

Figure 16 Stress concentration factor for trapezoidal riblets and various riblets angles

Effect of the riblet angle on the stress concentration factor

The influence of the riblet angle on the riblet stress concentration factor is analysed for round and trapezoidal notches, because these two shapes result in maximum and minimum stress concentration factors, respectively. Increasing the riblet angle leads to an increase in the stress concentration factor (figure 15). Because the radius of the circular arc, which connects both flanks of each groove, decreases for shallower riblet flanks, the notch sharpness increases and therefore the stress concentration factor increases as well.

Trapezoidal riblets show no clear trend in the stress concentration factor for increased riblet angles (figure 16). Thus, there is no clear conclusion which could be drawn for this case.

Effect of the beam height e.g. blade thickness on the stress concentration factor

The influence of the blade thickness on the stress concentration factor is analysed for trapezoidal riblets, based on the reference riblet geometry of (Lietmeyer, 2013). The following figures show the stress concentration factor for a beam/blade thickness of 0.50 mm and 0.25 mm, which are representative for the thin blade leading and trailing edges.

The stress concentration factor for a beam thickness of 0.50 mm is shown in figure 17. The maximum stress concentration factor in a single notch reaches 8.5. In comparison with figure 10, this value indicates that for a reduced blade thickness, there is a stress increasing influence from the opposite side of the blade. Surprisingly, for an increasing number of adjacent riblets, the stress concentration factor for thin airfoil sections converges fasters towards the limiting values of 7.77 and 2.93 for the end-notches and the central notches, respectively.

In the case that the blade thickness is further reduced to 0.25 mm, figure 18 shows that the maximum stress

concentration factor is further increased up to 8.51 by the notch interactions from the opposite blade side, and that the declining trend with increasing riblet number becomes even weaker.

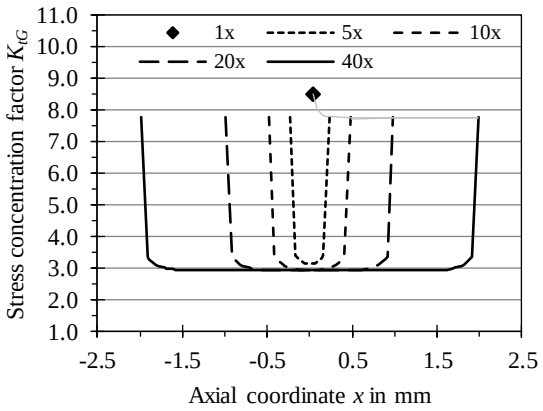

Figure 17 Stress concentration factor for a beam/blade thickness of 0.50 mm

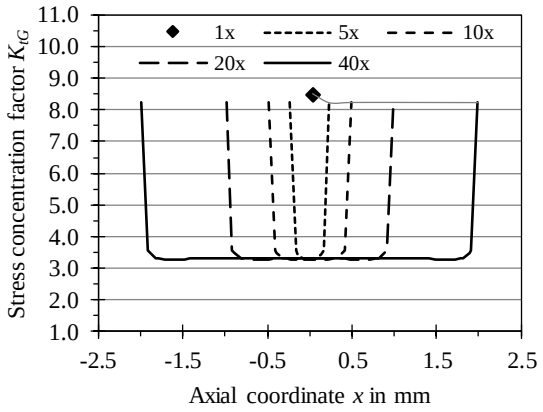

Figure 18 Stress concentration factor for a beam/blade thickness of 0.25 mm

Effect of adjacent riblet patches on the stress concentration factor

For a time- and cost-efficient structuring of the blade surface, it is favourable to group riblets of identical shape and dimensions into riblet patches. Since the riblet-parameters vary along the blade surface due to their dependency on local aerodynamic parameters like the wall shear stress, density, viscosity, and temperature, the blade surface will be covered by multiple versions of these patches.

Figure 19 Adjacent riblet patches

For this reason, the influence of adjacent riblet patches on their individual stress concentration factors is investigated. Trapezoidal notches with a width *s* of 100 µm and a depth *h* of 50 µm are used. Since aerodynamic interactions between adjacent riblet patches are rather unknown, there might be at least a mechanical reason to leave some unstructured space between adjacent patches. Thus, the influence of different distances between adjacent patches on the stress concentration factor is investigated (figures 20).

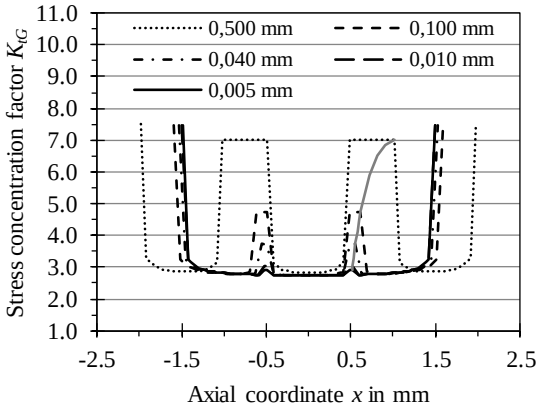

Figure 20 Stress concentration factor for adjacent riblet patches and various patch distances

Similar to what has been shown for previous configurations, the maximum stress concentration factor occurs in the end notches of each riblet patch. However, if neighbouring riblets patches and their respective end notches get closer to each other, the stress concentration factor of their respective end notches decreases. This effect spreads over the complete riblet patch with decreasing distance. This trend of decreasing notch effects continues until the adjacent riblet patches merge to one single riblet patch, when the end notches of the approaching patches become central notches after the patches merged into a single patch.

Conclusions on the influence of the riblet shape and dimensions on the notch effect

From an aerodynamic point of view, the trapezoid riblets have a higher potential for loss reduction than round or semi-circular riblets. However, especially the end notches of the trapezoidal notches lead to high stress concentration factors.

With this in mind, the concept of an optimized riblet configuration is developed. The aerodynamic consideration for this optimization is to include as many trapezoidal riblets in a riblet patch as possible, in order to profit from their superior aerodynamic performance. In order to minimize the maximum stress concentration factor of the end notches, the trapezoidal end notches are replaced by round or semi-circular end notches.

Figure 21 shows the results for this optimized riblet patch, which is combining trapezoidal notches at the patch center with round notches at the patch borders. It is obvious, that in the end notches there is a sharp drop in the stress concentration factor after this optimization. After this optimization, the highest stress concentration factor is limited by 2.81.

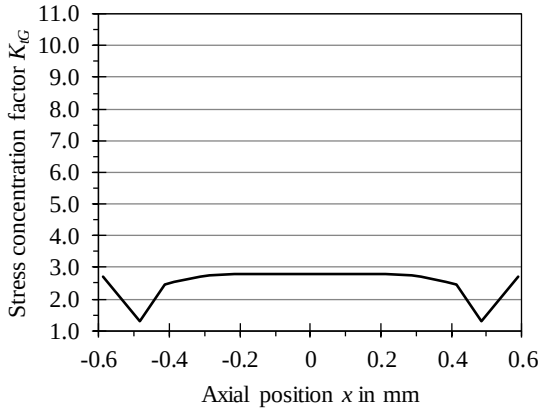

Figure 21 Optimized stress concentration factor for a riblet patch with trapezoidal riblets and round end-riblets

STRENGTH ANALYSIS OF RIBLET-STRUCTURED COMPRESSOR BLADES

Finally, the previous results served as a numerical basis for correlations between the riblet parameters and the stress concentration factor, which span wide parts of the riblet design space and allow for a fast prediction of the riblet notch effect during the design phase of a riblet structured compressor blade. Taking the stress results for the plain compressor blade and scaling the stresses by this correlated riblet notch effect yield the maximum stresses in the riblet structured blade.

For the sake of a safe blade design, the strength analysis can be conducted with the stress concentration factors from the end notches. Since the manufacturing of optimized riblet patches with shape-optimized end notches is currently cost-prohibitive, a single patch with a uniform riblet shape and dimensions is used in the following example. The result of the static stress analysis of this component is the loading level *a*. The loading level is an indicator for how much of the component strength is occupied by the loading. If this level is below 100%, the blade is sufficiently designed, it passes the numerical stress test, and it is unlikely to fail under static loading during operation under the assumed conditions.

The spanwise loading level for the second rotor blade, which is made from the material Ti6Al4V and structured with trapezoidal or round semi-circular riblets, is shown in figures 22 and 23. In each of these two cases, a complete coverage of the blade surface with riblets, which are manufactured by laser-ablation, is impossible due to strength limits.

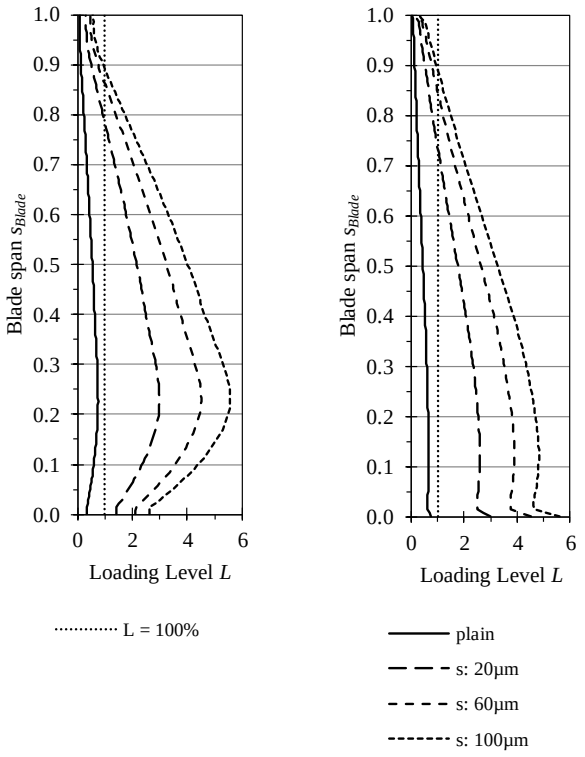

a) Pressure side **b) Suction side**

Figure 22 Loading level of a rotor blade structured with trapezoidal riblets

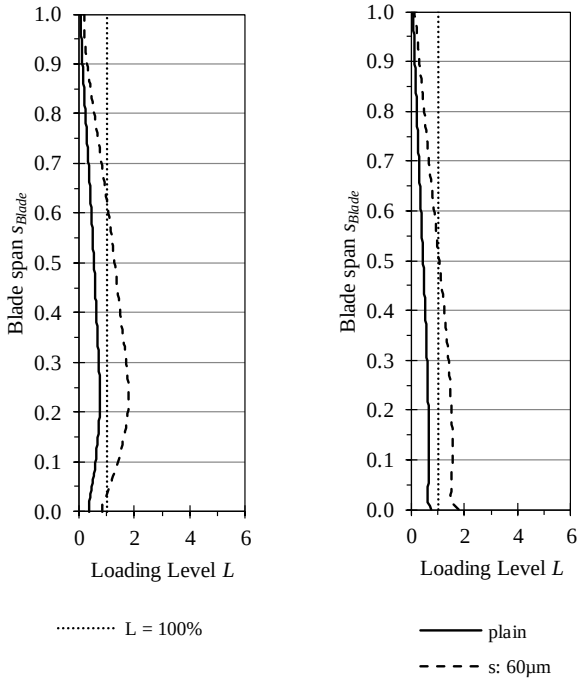

a) Pressure side **b) Suction side**

Figure 23 Loading level of a rotor blade structured with semi-circular riblets

In the case of trapezoidal riblets, the pressure and suction side can only be structured in the upper 21% and 25% of the blade span, respectively. When replacing the trapezoidal end notches by semi-circular groove shapes, up to 50% of the upper blade surface region might be structured with riblets.

For a further increase in the riblet-covered blade surface area the blade material, the blade shape or the rotational speed of an existing compressor design with smooth blade surfaces must be adopted, if riblets should be applied, which are manufactured without adding residual stresses to the blade body. Since in a first attempt, riblets are applied to an existing compressor design in order to improve its maximum performance under design conditions, reducing the operating speed is no option. The aerodynamic benefit from an increased blade thickness in order to increase the riblet-covered surface area has to be further evaluated against the increased profile loss from thicker airfoil sections.

CONCLUSIONS

Riblets, which are oriented perpendicular to the radial direction of the centrifugal forces of axial compressor rotor blades, form predetermined breaking points in the structured airfoil due to their stress-increasing notch effect. The influence of this notch effect can be determined by the stress concentration factor for various riblet design parameters. The smallest stress concentration factor can be achieved with riblets of a semi-circular notch shape, whereas the largest stress concentration factors result from trapezoid riblet shapes. An optimized mixed form with trapezoidal riblet in a patch, which is surrounded by semi-circular end notches is recommended for riblet-structured axial compressor blades.

The loading level in combination with the stress concentration factor can be used to identify the blade surface areas, which from a mechanical viewpoint can be covered with riblets, as well as those blade sections, which should be kept free from riblets. In the case of the compressor rotor blade presented here, structuring with exclusively trapezoidal riblets is only possible to a very limited extent of approximately the upper 20% of the blade span. When a patch of trapezoidal riblets is surrounded by semi-circular end-notches, up to 50% of the blade surface can be covered with riblets without an impermissible penalty on the blade integrity.

NOMENCLATURE

Variables

a	Width	mm
D	Sample thickness	mm
d	Notched sample thickness	mm
F	Force	N
h	Riblet height	µm
K_t	Stress concentration factor	-
L	Loading level	-
R_1	Notch radius	µm
R_k	Riblet tip radius	µm
r	Notch radius	µm
s	Riblet width	µm
s_{Blade}	Blade span	-
t	Notch depth	µm
x	Axial coordinate	mm
α	Riblet angle	°
β	Notch angle	°
σ	Normal stress	MPa

Indices

G	Gross
max	Maximum
N	Net
n	Nominal
p	Plain, smooth, free from notches

ACKNOWLEDGMENTS

The first author gratefully acknowledges the permission by the Institute of Turbomachinery and Fluid Dynamics to publish his thesis work.

REFERENCES

Bechert D.W., Bruse M., Hage W., van der Hoeven J.G.T., and Hoppe G. (1997). J. Fluid Mech., 338, 1997, pp. 59 – 8.

Bräunling, W.J.G. (2015). Flugtriebwerke, 4. Aufl., Springer Vieweg (VDI-Buch), Berlin.

Choi K.-S. (1990). Drag Reduction Test of Riblets Using Are's High Speed Buoyancy Propelled Vehicle-Moby-d," Aeron. J., 94(933), pp. 79–85.

Choi H., Moin P., and Kim J. (1993). Direct Numerical Simulation of Turbulent Flow over Riblets. J. Fluid Mech., 255, 1993, pp. 503 – 539.

Cumpsty N.A. (1998). Compressor Aerodynamics, Longman Group Ltd, Pearson Education Ltd, Harlow, Essex, U.K.

Daryusi, A. (2009). Beitrag zur Ermittlung der Kerbwirkung an Zahnwellen mit freien und gebundenem Auslauf, Dissertation, Technische Universität Dresden.

European Commission (2005). Flightpath 2050 Europe's Vision for Aviation, Luxembourg.

Grieb, H. (2009). Verdichter für Turbo-Flugtriebwerke, Springer Berlin Heidelberg.

Gümmer V. (2000). Pfeilung und V-Stellung zur Beeinflussung der dreidimensionalen Strömung in Leiträdern transsonischer Axialverdichter, Ph.D. thesis, Technische Universität München.

Hage W. (2004). Zur Widerstandsverminderung von Dreidimensionalen Riblet-Strukturen und Anderen Oberflächen. Ph.D. thesis, TU Berlin, Berlin.

Issler L., Ruoß H., and Häfele P. (2006). Festigkeitslehre – Grundlagen, Aufl. 2, Springer.

Jang P.S., Benney D.J., and Gran, R.L. (1986): On the Origin of Streamwise vortices in a turbulent boundary layer. J. Fluid Mech., 169, pp. 109 – 123.

Klocke F., Feldhaus B., Wegner H., and Bäcker V. (2010). J. Steel research Int. 81(9), 2010, pp. 178-181.

Klumpp S., Meinke M., and Schröder W. (2009): Proc. Turbulence and Shear Flow Phenomena 6, June 2009, Seoul, Korea.

Kordy H. (2015). Process abilities of the riblet-coating process with dual-cure lacquers. CIRP Journal of Manufacturing Science and Technology, Vol. 11, pp. 1-9.

Lietmeyer C., Chahine C., and Seume J. (2011). Numerical Calculation of the Riblet-Effect on Compressor Blades and Validation With Experimental Results, International Gas Turbine Congress, Osaka, Japan, Nov. 13–18, Paper No. IGTC2011-0106.

Lietmeyer C. (2013). Berechnungsmodell zur Widerstandsbeeinflussung nicht-idealer Riblets auf Verdichterschaufeln, Ph.D. thesis, Berichte aus dem Institut für Turbomaschinen und Fluid-Dynamik, Leibniz Universität Hannover, Hannover, Germany.

Lietmeyer C., Denkena B., Krawczuk T., Kling R., Overmeyer L., Wojakowsky B., Scheuer R., Vynnyk T., and Seume J. (2013). Recent Advances in Manufacturing of Riblets on Compressor Blades and Their Aerodynamic Impact. ASME J. Turbomach., 135(4), p. 041008.

McLean J., George-Falvy D., and Sullivan P. (1987). Flight Test of Turbulent Skin-Friction Reduction by Riblets," RAeS International Conference on Turbulent Drag Reduction by Passive Means, London, Sept. 15–17, pp. 408–424.

Monsarrat N., and Keenan M. (1967). Experimental Analysis of Transonic Stators, Pratt & Whitney Aircraft.

Niemann G., Winter H., and Höhn B-R. (2001). Maschinenelemente, Band 1, Aufl. 3, Springer.

Oehlert K., and Seume J (2006). Exploratory Experiments on Machined Riblets on Compressor Blades. 2nd Joint U.S. European Fluids Engineering Division Summer Meeting, ASME Paper No. FEDSM2006-98093.

Oehlert K., Seume J., Siegel F., Ostendorf A., Wang B., Denkena B., Vynnyk T., Reithmeier E., Hage W., Knobloch K., and Meyer R. (2007). Exploratory Experiments on Machined Riblets for 2-D Compressor Blades. ASME Paper No. IMECE2007-43457.

Romans T., Thome M., and Hirt G. (2009): Riblet Rolling. International Aluminium Journal 85, 7/8, pp 54-56.

Romans T., and Hirt G. (2010): Rolling of Drag Reducing Riblet Surface. 51st AIAA/ASME/ASCE/AHS/ ASC Structures, Structural Dynamics & Materials Confe-rence, 12 - 15 April 2010, Orlando, Florida.

Romans T. (2014). Development and analysis of the Riblet Rolling Process, Ph.D. thesis, Rheinisch-Westfälische Technische Hochschule Aachen.

Sawyer W., and Winter K.. (1987). An Investigation of the Effect on Turbulent Skin Friction of Surfaces With Streamwise Grooves. International Conference on Turbulent Drag Reduction by Passive Means, London, Sept. 15–17, pp. 330A–362.

Squire L., and Savill, A. (1987). Some Experiences of Riblets at Transonic Speeds, RAeS International Conference on Turbulent Drag Reduction by Passive Means, London, Sept. 15–17, pp. 392–407.

Young W.C., and Budynas R.G. (2002). Roark's Formulas for Stress and Strain, 7th edition, McGraw-Hill.

APPENDIX – MATERIAL PROPERTIES

			Ti6Al4V 3.7165	EN AW 7075 3.4365
Density	ρ	[kg/m³]	4430	2800
Young's modulus	E	[MPa]	114.000	71.000
Ultimate strain	A	[%]	10	8
Ultimate tensile strength	R_m	[MPa]	895	540
Yield stress	R_p	[MPa]	828	485